analytical chemistry

Article

pubs.acs.org/ac

Dye-Sensitized and Localized Surface Plasmon Resonance Enhanced Visible-Light Photoelectrochemical Biosensors for Highly Sensitive Analysis of Protein Kinase Activity

Zhiyong Yan,[†,‡] Zonghua Wang,[*,†] Zhuang Miao,[§] and Yang Liu[*,‡]

[†]Laboratory of Fiber Materials and Modern Textile, The Growing Base for State Key Laboratory, College of Chemical Science and Engineering, Shandong Sino-Japanese Center for Collaborative Research of Carbon Nanomaterials, Qingdao University, Qingdao, Shandong 266071, China

[‡]Department of Chemistry, Beijing Key Laboratory for Analytical Methods and Instrumentation, Key Laboratory of Bioorganic Phosphorus Chemistry & Chemical Biology of Ministry of Education, Tsinghua University, Beijing 100084, China

[§]Departments of Neurosurgery, China-Japan Union Hospital of Jilin University, Changchun, Jilin 130033, China

Supporting Information

ABSTRACT: A novel visible-light photoelectrochemical (PEC) biosensor based on localized surface plasmon resonance (LSPR) enhancement and dye sensitization was fabricated for highly sensitive analysis of protein kinase activity with ultralow background. In this strategy, DNA conjugated gold nanoparticles (DNA@AuNPs) were assembled on the phosphorylated kemptide modified TiO_2/ITO electrode through the chelation between Zr^{4+} ions and phosphate groups, then followed by the intercalation of $[Ru(bpy)_3]^{2+}$ into DNA grooves. The adsorbed $[Ru(bpy)_3]^{2+}$ can harvest visible light to produce excited electrons that inject into the TiO_2 conduction band to form photocurrent under visible light irradiation. In addition, the photocurrent efficiency was further improved by the LSPR of AuNPs under the irradiation of visible light. Moreover, because of the excellent conductivity and large surface area of AuNPs that facilitate electron-transfer and accommodate large number of $[Ru(bpy)_3]^{2+}$, the photocurrent was significantly amplified, affording an extremely sensitive PEC analysis of kinase activity with ultralow background signals. The detection limit of as-proposed PEC biosensor was 0.005 U mL^{-1} ($S/N = 3$). The biosensor also showed excellent performances for quantitative kinase inhibitor screening and PKA activities detection in MCF-7 cell lysates under forskolin and ellagic acid stimulation. The developed dye-sensitization and LSPR enhancement visible-light PEC biosensor shows great potential in protein kinases-related clinical diagnosis and drug discovery.

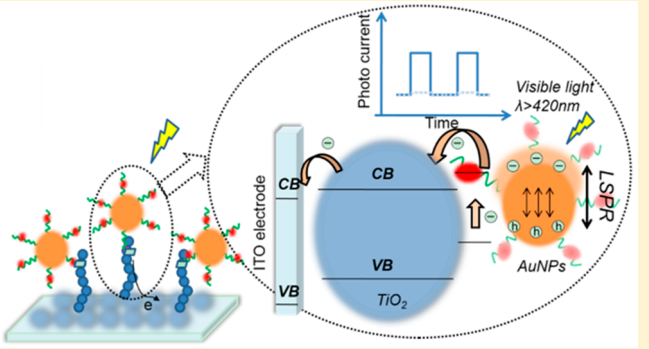

Protein phosphorylation by kinases plays important regulatory roles in diverse cellular functions including the regulation of metabolism,[1] gene transcription,[2] cell cycle progression,[3] and apoptosis.[4] About a third of mammalian proteins contain covalently bound phosphate and there may be 2000 protein kinases and 500 protein phosphatases encoded by the human genome.[5] Deregulated protein kinase activity (overexpression in most cases) and abnormal protein phosphorylation states are closely associated with many diseases, such as Alzheimer's diseases, cancers, and diabetes, etc.[6−9] Protein kinase has been used as important biomarkers for diseases diagnostic and emerged as targets for treatment of a number of diseases by using kinase inhibitors to down-regulate the activities of related protein kinase.[10,11] As a result, accurate measurement of protein kinase activity and their potential inhibitors screening is not only helpful for the clinical diagnosis and targeted therapy, but also necessary for further understanding the molecular mechanism of signal transduction. Thus, rapid and sensitive assays for determining protein kinase activity are urgently needed.

Up to now, several techniques have been developed for protein kinase activity detection including radiometric assays,[12] fluorescence,[13] chemiluminescence,[14−16] mass spectrometry,[17] etc.[18−21] Although these methods mentioned above have their own unique advantages, such as high specificity, rapidity, low sample volume, and real-time monitoring, etc.[22] However, most of them suffer from certain drawbacks such as harmful radioactive labels, sophisticated instrumentation, complicated operations or nonignorable back signal. Recently, photoelectrochemical (PEC) approach has captured considerable attention because it contains the merits of electrochemical and optical assay.[23−31] By using photoirradiation coupled with

Received: September 28, 2015
Accepted: November 25, 2015

DOI: 10.1021/acs.analchem.5b03661
Anal. Chem. XXXX, XXX, XXX−XXX

electrochemical detection, the PEC method is very sensitive with greatly reduced background signals.[32−34] What's more, advantageously inherited from the electrochemical method, the PEC instrument is simple, inexpensive and easy to miniaturization compared with conventional optical detection methods.[35−37] The performance of PEC biosensors is largely influenced by the photo-to-current conversion efficiency of photoactive materials used in the biosensors. Recently, quantum dots (QDs) incorporation and dyes sensitization have been investigated to improve the photocurrent conversion efficiency of the PEC biosensors.[38,39] Photoactive materials (such as TiO_2, ZnO) incorporate with QDs which possess cascade band-edge levels can not only enhance the utilization of light energy but also reduce the electron−hole recombination. For example, a CdS QDs sensitized TiO_2 photoelectrode was developed for cardiac marker troponin T detection by the charge separation in CdS QDs and photocurrent production upon illumination.[40] A PEC biosensor based on two different sizes of CdTe QDs cosensitized TiO_2/CdS:Mn hybrid structure was designed for DNA detection, in which the CdTe QDs with two different sizes promoted the long-wavelength light and middle-wavelength light harvest and Mn^{2+} reduced the electron recombination of photo generated electrons.[41] Though great progress has been achieved by using QDs sensitization strategies, QDs have several inherent drawbacks such as their sensitivity toward hydrolysis and oxidation, high demands on the crystallinity of the material, and toxic constituents.[42] Besides, the synthesis process of quantum dots is very strict and complicated.[43] As an alternative way, dyes sensitization is another strategy to improve the light harvest ability and photocurrent production in solar cells.[44−46] However, the weak adsorption of dyes on the semiconductor layers limited their applications in highly sensitive biosensors development.

Due to the collective oscillating conduction electrons driven by the applied electromagnetic field of incident light, noble metal nanoparticles exhibit localized surface plasmon resonance (LSPR). LSPR brings the noble metal nanoparticles several unique benefits, such as the unique plasmon absorbance features, intensive localized electric field in the vicinity and visible light-induced charge separation occurred at the surface.[47] Recently, PEC biosensors based on LSPR have been a hot topic drawing a lot of research interests.[48−51] The LSPR of AuNPs can not only act as light harvesting antennae for dye that improves the light harvest ability, and but also enhance the photocurrent transfer efficiency, which make it promising in the development of biosensor with high performances.[52,53]

In this work, a novel and highly sensitive turn-on PEC platform for kinase activity assay and inhibitor screening was developed based on AuNPs LSPR signal amplification and dye sensitization strategy. In this strategy, TiO_2 was first fabricated on the ITO electrode, followed by the modification of kemptide. Then the kemptide on the electrode was phosphorylated in the presence of protein kinase A (PKA) using adenosine triphosphate (ATP) as a coreactor. DNA conjugated gold nanoparticles (DNA@AuNPs) probes were fabricated and specifically adsorbed on the electrode based on the coordination of Zr^{4+} ions with phosphate groups on DNA and phosphorylated kemptide, followed by the intercalation of $[Ru(bpy)_3]^{2+}$ in the grooves of DNA on the probes.[54] When the fabricated electrode was exposed on the visible light, a sharp photocurrent produced owing to LSPR signal amplification and dye sensitization, and can be applied for highly sensitive PKA activity detection with ultralow background. Moreover, kinase inhibitor screening and kinase activities evaluation in complicated cell lysates samples stimulated by ellagic acid and forskolin were also conducted. This strategy provides a sensitive and robust platform for kinase activity assay, and is potential in the applications of clinic diagnostic and drug discovery.

EXPERIMENTAL SECTION

Materials and Reagents. PKA (catalytic subunit from bovine heart), Tris(2,2′-bipyridyl) dichlororuthenium(II) hexahydrate ($Ru(bpy)_3Cl_2•6H_2O$, $[Ru(bpy)_3]^{2+}$), 4,4′,5,5′,6,6′-hexahydroxydiphenic acid 2,6,2′,6′-dilactone (Ellagic acid), N-(3-chlorophenyl)-6,7-dimethoxy-4-quinazolinamine (Tyrphostin AG1478), Forskolin and 3-isobutyl-1-methylxantine (IBMX) were purchased from Sigma. Cysteine-terminated kemptide (CLRRASLG) was obtained from GL Biochem (Shanghai, China). DNA1 (5′-SH-C6-ATCGTTTAGGATTTGGATGA-P-3′), DNA2 (3′-GCAAATCCTAAAC) were synthesized and purified by Sangon Inc. (Shanghai, China). ATP was obtained from Dingguo Biological Products Company (China). Other regents of analytical grade were provided from Beijing Chemical Company (China). $HAuCl_4·3H_2O$ (48% w/w) was obtained from Shanghai Reagent (Shanghai, China).

Preparation of DNA@AuNPs Nanoprobes. AuNPs were prepared as reported previously.[55] In brief, 100 mL of 0.01% (w/v) $HAuCl_4$ solution was boiled with vigorous stirring, and 0.5 mL of 1% (w/v) trisodium citrate solution was quickly added into the boiling solution. Wine red solution was obtained, indicating the formation of AuNPs which were characterized (Figure S-1 in Supporting Information). The DNA@AuNPs nanoprobes were prepared by adding the double-stranded DNA hybrid of DNA1 and DNA2 into 1 mL of gold colloidal solution. After stirring for 24 h, 150 μL of 1 M NaCl was added. Finally, the mixture was centrifuged at 12 000 rpm for 15 min twice, and then dispersed in buffer solution (pH 7.4) containing 300 mM NaCl and 50 mM Tris-HCl. The DNA@AuNPs nanoprobes were characterized by UV−vis spectra (Figure S-1A in the Supporting Information). The characteristic absorption peak of AuNPs was red-shifted from 529 to 533 nm after the decoration of double-stranded DNA, indicating the successfully hybridization of DNA on the surface of AuNPs. According to the Nanodrop spectrophotometer, it was calculated that about 450 double-stranded DNA hybrids were loaded on each 46 nm AuNPs, which could act as an excellent carriers for $[Ru(bpy)_3]^{2+}$ molecules, and the $[Ru(bpy)_3]^{2+}$/AuNPs ratio was around 7650:1.

Phosphorylation of Kemptide on ITO Slices. The ITO slices were sonicated in acetone, NaOH (1 M) in 1:1 (v/v) ethanol/water, and water consequently. Then the clean-washed ITO slices were dried in the oven at 90 °C for 12 h. A series of 1.5 mg × mL^{-1} TiO_2 suspensions were drop-coated on ITO slices with the fixed area (0.5 cm^2). The modified ITO slices were heated at 200 °C for 15 h, following by the irradiation of ultraviolet ozone for 30 min. After drying in an N_2 atmosphere, the TiO_2/ITO slices were silanized in a 5 wt % acetone aqueous solution of 3-(aminopropyl triethoysilane) (APTES). After being cleaned with acetone, the amino-silane grafted TiO_2/ITO slices were dried at 110 °C for 1 h. Prior to immobilization of kemptide, the silanized ITO slices were immersed in glutaraldehyde solutions for 1 h, then the electrode was cleaned and immersed into a PBS (10 mM, pH 7.4) solution containing 500 μM cysteine terminated kemptide

DOI: 10.1021/acs.analchem.5b03661
Anal. Chem. XXXX, XXX, XXX−XXX

Scheme 1. Configuration of Photoelectrochemical Biosensor for Kinase Activity Detection

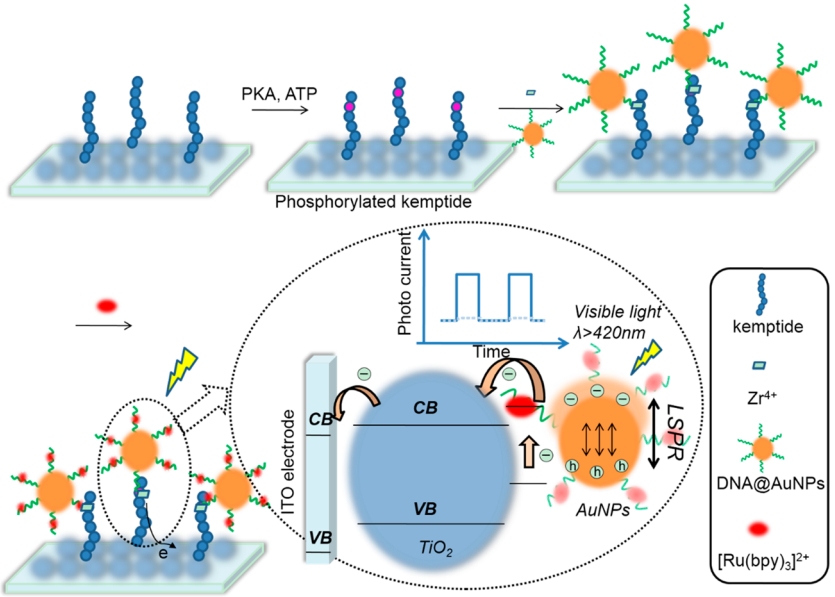

for 12 h in darkness. Then the kemptide was immobilized on TiO_2/ITO slices through the reaction between the amino group on the kemptide and aldehyde group of the glutaraldehyde. After that, the electrode was washed thoroughly with PBS solution (1 mM, pH 7.4), followed by immersing in 1 mM 6-aminohexanoic acid solution for 30 min at ambient temperature to avoid the nonspecific binding. A PKA-catalyzed phosphorylation reaction was performed by incubating the modified electrode in a PBS solution (50 mM Tris-HCl and 20 mM $MgCl_2$, pH 7.4) containing a desired amount of PKA and ATP at 37 °C. After that, the electrode was rinsed to remove the excess reagents. The phosphorylated peptide modified electrode was then treated in 0.5 mM Zr^{4+} solution at room temperature, followed by rinsing absolutely with blank PBS and double distilled water. After being dried with N_2, the electrode was incubated in the solution containing DNA@AuNPs. After that, the resulted electrode was thoroughly washed to remove the nonspecific DNA@AuNPs, and was immersed in 50 μM $[Ru(bpy)_3]^{2+}$ solution for 10 min and then washed three times for photocurrent characterization. For the PKA inhibition and cell lysates assay, the procedures were similar to those above, except that different concentrations of inhibitor or cell lysates were added in the PKA reaction mixture.

Preparation of MCF-7 Cell Lysates. MCF-7 cells were cultured in DMEM medium supplement at 37 °C under a humidified atmosphere containing 5% CO_2. The culture medium was replaced by serum-free medium (1 mL) for 4 h before stimulation. Subsequently, the cells were treated with desired concentrations of adenylyl cyclase activator of Forskolin and IBMX solutions and PKA inhibitor ellagic acid, with final concentration at 25 μM, respectively. After that, the cultured cells were treated with 2 mL of lysis buffer for 5 min, and then the cell lysates were clarified. Finally, the resulting supernatants were stored at −80 °C and were ready for PKA activity detection.

The PKA activity detection in cell lysates was performed by diluting the cell lysates into desired volumes of PKA assay buffer (50 mM Tris-HCl, 20 mM $MgCl_2$, 100 μM ATP, pH 7.4). The fabrication and measurement protocols were set by the same procedure with above.

Apparatus and Characterization. All photocurrent experiments were carried on a conventional three-electrode system with a CHI802B electrochemical workstation (Chenhua Instrument Company of Shanghai, China) using the modified electrode as working electrode, and platinum wire and Ag/AgCl with saturated KCl solution were used as counter electrode and reference electrode, respectively. Electrochemical impedance spectroscopy (EIS) was conducted on SP-150 (PARSTAT2273. USA) in a solution containing 5 mM $K_3[Fe(CN)_6]/K_4[Fe(CN)_6]$ and 0.1 M KCl in the frequency range from 0.1 to 100 kHz. The UV−vis absorption spectra were performed with a UV-3900 spectrophotometer (Hitachi, Japan). SEM images were obtained with a Hitachi SU8010 (Hitachi, Japan). The concentration of DNA was measured with a NANODROP 2000 spectrophotometer (Thermo scientific). PEC measurement were irradiated with visible light (λ > 420 nm) using a xenon lamp as light source. Desired action spectra were collected using a xenon lamp with an appropriate band-pass filter.

RESULTS AND DISCUSSION

Protein Kinase Activity Evaluation by LSPR Enhanced Dye Sensitized PEC strategy. Scheme1 describes the configuration of the PEC biosensor for kinase activity analysis. The cysteine-terminated kemptides were first assembled on the TiO_2/ITO electrode. Then, 6-aminohexanoic acid was further modified on the electrode as blocking reagent to avoid nonspecific adsorption. In the presence of PKA, the serine of substrate peptide was phosphorylated in the presence of PKA and the phosphorylated peptide captured the DNA@AuNPs by the multicoordinative interaction between Zr^{4+} and the intrinsic 3′-phosphate end of DNA. Owing to the large surface area of AuNPs, a majority of DNA were conjugated on AuNPs, and thus a large number of $[Ru(bpy)_3]^{2+}$ molecules were absorbed by inserting into the grooves of the DNA probes. When the fabricated electrode was exposed under the visible light, $[Ru(bpy)_3]^{2+}$ molecules can harvest visible light to produce excited electrons that inject into the TiO_2 conduction band to form the photocurrent. At the same time, oscillating electric fields localized in the vicinity of the AuNPs were generated,

DOI: 10.1021/acs.analchem.5b03661
Anal. Chem. XXXX, XXX, XXX−XXX

which can enhance the photocurrent by exciting electrons of $[Ru(bpy)_3]^{2+}$ molecules (e.g., HOMO−LUMO transition).[53] What's more, AuNPs derived a collective oscillation of free electrons under the visible light and the photo injected electrons can also be driven from AuNPs into the TiO_2 conduction band directly, thus the photocurrent was further amplified. Besides, the photocurrent signal is also benefited from the large surface area and excellent conductivity of AuNPs that capture more $[Ru(bpy)_3]^{2+}$ molecules and facilitate the electron transfer at the electrode interface. Therefore, the as-designed PEC biosensor provides a sensitive tool for kinase activity evaluation.

Characterization of the Kemptide Modified TiO_2/ITO Electrode. EIS was applied to characterize the assembly processes of the electrode using $[Fe(CN)_6]^{4-/3-}$ as electroactive probes. In the Nyquist plot, the diameter of the semicircle at higher frequency range is equal to the R_{et}, which represents the electron transfer kinetics of the electroactive probes at the electrode interface.[56] As shown in Figure 1, the

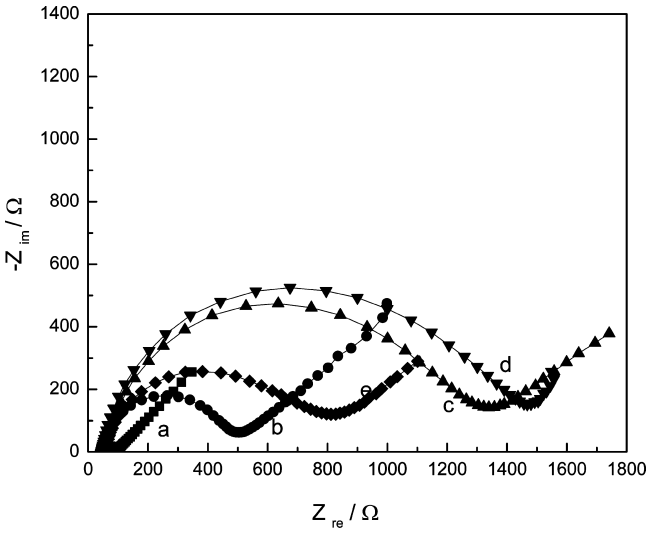

Figure 1. (A) Electrochemical impedance spectroscopy of (a) the bare ITO electrode, (b) TiO_2/ITO, (c) kemptide/TiO_2/ITO, (d) phosphorylated kemptide/TiO_2/ITO, (e) $[Ru(bpy)_3]^{2+}$/DNA@AuNPs/phosphorylated kemptide/TiO_2/ITO. The spectra were recorded in $Fe(CN_6)^{3-/4-}$ solution in the frequency range from 0.1 Hz to 100 kHz.

bare ITO electrode exhibits the small R_{et} value (curve a). After the modification of TiO_2, the R_{et} increased obviously (curve b). When the TiO_2/ITO electrode was assembled with kemptide (curve c) and then phosphorylated by PKA (curve d), the diameter of semicircle successively increased, suggesting the decrease of electron transfer rate on the electrode interface. This was attributed to the electron inert feature of kemptide, and that the replacement of hydroxide group by phosphate group increased the negative charge density of kemptide and hindered the electron transfer at the electrode interface. As a while, the R_{et} value decreased obviously after the electrode was treated with Zr^{4+} ions and $[Ru(bpy)_3]^{2+}$ embedded DNA@AuNPs ($[Ru(bpy)_3]^{2+}$/DNA@AuNPs) (curve e), attributing to the excellent conductivity of AuNPs that facilitated electron-transfer on the electrode interface. The surface density of immobilized kemptide on the electrode was studied by EIS. The surface coverage (θ_E) of kemptide on the electrode was calculated to be 65% according to the equation below:

$$\theta_{E\text{kemptide}} = (1 - R_{et}/R_{et}^{\text{kemptide}}) \times 100\% \quad (1)$$

where R_{et} is the charge transfer resistance of the TiO_2 surfaces, and R_{et}^{kemptide} is the corresponding resistance of kemptide immobilized surfaces.[57,58]

PEC Behaviors of the Biosensor. The PEC behaviors of the modified electrode were studied by the photocurrent transient technique. Figure 2A presents the photocurrent responses of the modified ITO electrode in 0.1 M PBS containing 0.1 M ascorbic acid under visible light irradiation. It was observed that both the ITO and TiO_2/ITO electrodes exhibited negligible photocurrent response under visible light. When the TiO_2/electrode was treated with kemptide, and then was phosphorylated by PKA, there was nearly no photocurrent response. However, when $[Ru(bpy)_3]^{2+}$/DNA@AuNPs nanoprobes were assembled on the phosphorylated kemptide modified electrode, a sharply increased photocurrent response was found due to the injection of electrons both from the $[Ru(bpy)_3]^{2+}$ molecules excited by LSPR and the irradiated AuNPs to the conduction band of TiO_2.

To testify the photocurrent response of the $[Ru(bpy)_3]^{2+}$/DNA@AuNPs probes conjugated phosphorylated kemptide, a series of controlled experiments were conducted. The photocurrents responses of the modified electrodes treated with and without PKA catalysis were recorded. Figure 2B shows the photocurrent response on the phosphorylated kemptide (curve a) and kemptide (curve b) with the treatments of $[Ru(bpy)_3]^{2+}$/DNA@AuNPs multicoordinated by Zr^{4+}. It was noted that the kemptide modified electrode without PKA catalysis exhibited a very weak photocurrent signal that could be ignored. This is because the kemptide cannot be phosphorylated in the absence of PKA, thus failed to capture $[Ru(bpy)_3]^{2+}$/DNA@AuNPs. While after the phosphorylation by kinase, a strong photocurrent signal was observed due to the modification of $[Ru(bpy)_3]^{2+}$/DNA@AuNPs. To demonstrate the meliority of the biosensor, the photoelectrodes with Zr^{4+} coordinated phosphorylated kemptide were treated with DNA, $[Ru(bpy)_3]^{2+}$ modified DNA, DNA@AuNPs and $[Ru(bpy)_3]^{2+}$/DNA@AuNPs respectively and the photocurrent responses were shown in Figure 2C. It was clear that the electrode treated with DNA presented negligible photocurrent signals under visible light irradiation. In addition, the photocurrent signals of the electrode treated with $[Ru(bpy)_3]^{2+}$ intercalated DNA was also very weak. The facts demonstrate that less amount of DNA were adsorbed on the electrode, and the photocurrent response was very weak even though $[Ru(bpy)_3]^{2+}$ had obvious adsorption in the visible light range. In addition, when the kemptide modified electrode was treated with AuNPs, the photocurrent response was also negligible owing to the weak adsorption of gold nanoparticles on the peptide modified electrode (Figure S-2 in the Supporting Information). While the photocurrent signal of the phosphorylated photoelectrodes treated with the DNA@AuNPs probes showed a slight increase (curve c), which could come from the photoinjected electrons of AuNPs to the conduction band of TiO_2. However, the photocurrent signal intensities for all above cases were much weaker than that of the $[Ru(bpy)_3]^{2+}$/DNA@AuNPs modified electrode (curve d). To clarify the significant increase of the photocurrent from the $[Ru(bpy)_3]^{2+}$/DNA@AuNPs probes, the normalized photocurrent action spectrum were characterized (Figure S-3 in the Supporting Information). The results indicated that the photocurrent of the electrode conjugated with $[Ru(bpy)_3]^{2+}$/

DOI: 10.1021/acs.analchem.5b03661
Anal. Chem. XXXX, XXX, XXX−XXX

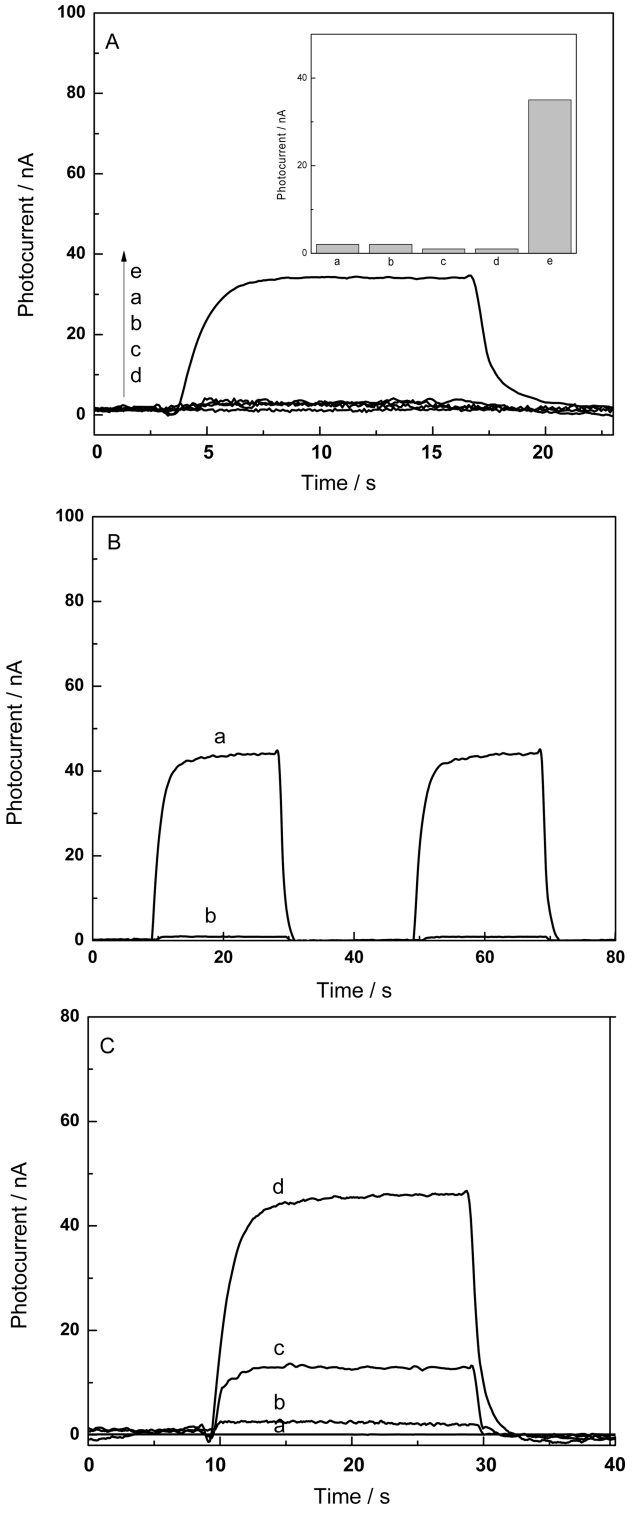

Figure 2. PEC behaviors of the biosensors. (A) The transient photocurrent responses of (a) the bare ITO electrode, (b) TiO_2/ITO, (c) kemptide/TiO_2/ITO, (d) PKA catalyzed phosphorylated kemptide/TiO_2/ITO, (e) $[Ru(bpy)_3]^{2+}$/DNA @ AuNPs/phosphorylated kemptide/TiO_2/ITO. (B) The photocurrent response on the kemptide (a) and phosphorylated kemptide with the treatments of $[Ru(bpy)_3]^{2+}$/DNA@AuNPs structure (b). (C) The photocurrent of phosphorylated kemptide modified electrode with the treatment of (a) DNA double strand, (b) $[Ru(bpy)_3]^{2+}$ modified DNA, (c) DNA@AuNPs and (d) $[Ru(bpy)_3]^{2+}$/DNA@AuNPs. The light power density is 190 mW cm^{-2}, electrode area is 0.5 cm^2.

DNA@AuNPs probes is generated by the transition of electrons from $[Ru(bpy)_3]^{2+}$ to the TiO_2 conduction band, which can be amplified by the LSPR induced localized electric fields of AuNPs. In addition, the injection of the free electrons from the AuNPs to the TiO_2 conduction band under light irradiation also contributes the photocurrent generation. What's more, it is noted that the AuNPs can not only increase the interface area of the modified electrode to capture more $[Ru(bpy)_3]^{2+}$ molecules but also facilitate the electron transfer at the electrode interface. As a result, the photocurrent is significant improved. Accordingly, the as-proposed strategy provides a simple and sensitive platform for kinase activity assay and inhibitor screening.

Optimization of the Detection Conditions. LSPR is greatly influenced by the size of AuNPs, for the electronic structure change dramatically with different AuNPs. Figure S-4 shows the size dependent photocurrent in this strategy. The photocurrent was increased with the increasing diameter of AuNPs, which can be ascribed to the fact that the larger size of AuNPs exhibits stronger localized electric fields and generates larger photocurrent.[59] Besides, the AuNPs with large size can facilitate the excitation and movement of free electrons.[51] However, the larger gold nanoparticles present worse stability, thereby, AuNPs with 46 nm were chosen for our experiment.

ATP offers the phosphate groups during the phosphorylation reaction. As shown in Figure S-5A in the Supporting Information, the photocurrent change of the kemptide modified electrode increased with the increasing concentrations of ATP and reached a maximal value at the ATP concentration of 100 μM, then it maintained the intensity at higher concentration of ATP. The facts manifested that 100 μM ATP was sufficient to the phosphorylation reaction catalyzed by PKA. Thus, the optimal concentration of ATP was 100 μM.

The phosphorylation time is an important parameter for the kinase-catalyzed reaction on the electrode surface. From Figure S-5B, with the increase of the incubation time, the photocurrent signal increased and then reached a plateau in 80 min, indicating a tendency to complete phosphorylation of kemptide. Therefore, the optimal phosphorylation time was 80 min. In addition, the temperature of enzyme catalyzed reaction was also investigated. The optimal temperature for the phosphorylation procedure of kemptide by PKA was 37 °C in these experiments (Figure S-5C in the Supporting Information).

PEC Measurements of PKA Activity. The activity of protein kinase was evaluated with different concentrations of PKA under the optimized experimental conditions. Figure 3 shows the changes of the photocurrent as a function of PKA activity. The photocurrent increased accordingly with the increase of PKA activity and reached a platform value after 80 U mL^{-1}. As shown in the inset of Figure 3B, the photocurrent was proportional to the logarithm value of PKA concentration in the range from 0.008 U mL^{-1} to 1 U mL^{-1} with a correlation equation of $I = 45.3 + 18.9 \times \log c$ with the correlation coefficient of $R = 0.996$, where I was the photocurrent intensity and c was the kinase activity. The detection limit of PKA was calculated to be 0.005 U mL^{-1} (S/N = 3), which showed obviously excellent performance compared with the previous reported assays (Table S-1, Supporting Information). The high sensitivity can be attributed to the following reasons. Under visible light irradiation, the adsorbed $[Ru(bpy)_3]^{2+}$ molecules can harvest visible light to produce excited electrons that inject into the TiO_2 conduction band to form the photocurrent,

DOI: 10.1021/acs.analchem.5b03661
Anal. Chem. XXXX, XXX, XXX−XXX

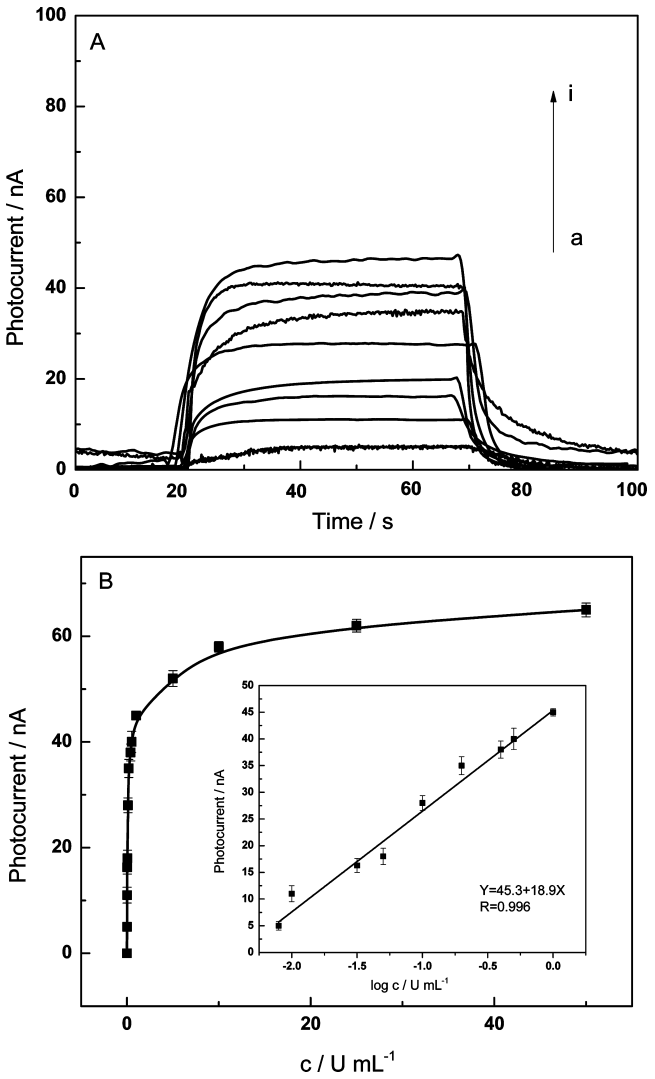

Figure 3. (A) The photocurrent intensity of different PKA concentrations: 0.008 U mL^{-1} (a), 0.01 U mL^{-1} (b), 0.03 U mL^{-1} (c), 0.05 U mL^{-1} (d), 0.1 U mL^{-1} (e), 0.2 U mL^{-1} (f), 0.4 U mL^{-1} (g), 0.5 U mL^{-1} (h), 1 U mL^{-1} (i). (B) The photocurrent change of different PKA concentrations ranging from 0 to 50 U mL^{-1}. The inset is the linear relationship between current intensity and the logarithm value of PKA concentration. The light power density is 190 mW cm^{-2}, electrode area is 0.5 cm^2.

meanwhile, the photocurrent efficiency was further improved by intensive localized electric field of AuNPs. Besides, free electrons from the irradiated AuNPs can inject directly into the TiO_2 conduction band, which can also enhance the photocurrent. Finally, AuNPs facilitated electron-transfer at interface of the electrode and accommodate large number of $[Ru(bpy)_3]^{2+}$, thus the photocurrent was significantly amplified. This demonstrates that the proposed PEC method can be employed for highly sensitive kinase activity detection.

Repeatability of this biosensor assessed by assaying the same level of PKA activity of 1 U mL^{-1} with 12 independently fabricated biosensors. The relative standard deviation (RSD) is 8%, demonstrates acceptable repeatability. What's more, the stability of the designed biosensor was also evaluated by assaying the PKA activity of 1 U mL^{-1} with one freshly prepared electrode, and the RSD was 2.3%, indicating the good stability of the biosensor.

Kinase Activity Inhibition Evaluation and Detection in Cell Lysates. The screening of potential inhibitors of protein kinase is of great significance in drug discovery.[60] To demonstrate the potential application of in the inhibition assay, the kinase activities were measured with different concentrations of kinase inhibitors. As shown in Figure 4A, the change of the photocurrent was recorded in the presence of ellagic acid, a cell-permeable inhibitor of PKA. The current intensity decreased along with the increasing concentrations of ellagic acid and then reached a stable level when the concentrations of ellagic acid were over 10 μM. The half-maximal inhibition values (IC_{50}) was calculated to be 3.01 μM, which is comparable with our previous result.[61] In addition, the PKA activity analysis was also conducted in the presence of Tyrphostin AG 1478 which is a tyrosine kinase inhibitor but not a PKA inhibitor. As seen in curve b of Figure 4A, the photocurrent signal had negligible changes with the concentration change of Tyrphostin AG 1478. These results indicated that the as-designed PEC biosensor is potential in quantitative kinase inhibitors screening.

Deregulated expression of PKA caused by extra stimulation has been associated with a series of cellular problem such as cell proliferation and neoplastic transformation, besides, PKA is also served as a cancer biomarker for diagnostics and prognostics. The activation and inhibition of the intracellular PKA from MCF-7 Cell line with the treatment of Forskolin combined with IBMX and ellagic acid respectively were measured by the PEC biosensor. As shown in Figure 4B, it was observed that the MCF-7 cells treated with ellagic acid exhibited lowest PKA activity of 0.008 UmL^{-1}, and it was lower than that of the controlled cell line without stimulations of 0.02 UmL^{-1}. The MCF-7 cell line treated with Forskolin exhibited the highest level of PKA among these samples. The results were also comparable with those by ELISA measurements (Figure S-6 in the Supporting Information). What's more, MCF-7 cells were stimulated with different concentrations of forskolin and IBMX for PKA activation. The PKA activities in cell lysates were evaluated and the results were shown in Figure 4C. The photocurrent increased with the increasing concentrations of Forskolin and IBMX. An initial quick increase followed by a slow increase in both samples was observed in the range from 0 to 25 μM. These results indicate that the sensing platform is available for in vitro cell kinase assay.

CONCLUSIONS

In conclusion, a LSPR enhanced and dye-sensitized turn-on PEC biosensor has been developed for kinase activity and inhibition assay. The photocurrent generated on the $[Ru(bpy)_3]^{2+}$ sensitized TiO_2 photoelectrode under visible light irradiation was greatly enhanced by LSPR induced localized electric fields of AuNPs. Together with the excellent conductivity and large surface area properties of AuNPs, the signal-to-noise ratio and sensitivity of the PEC biosensor are greatly enhanced with an ultralow background. A detection limit of 0.005 UmL^{-1} was obtained under visible light illumination. The PEC biosensor also shows excellent performance on quantitative kinase inhibitor screening and PKA activities detection in complicated cell lysates samples. Therefore, with its simplicity, sensitivity and practicality in cell lysate assay, the present work not only provides a sensitive platform for other kinase activity assay and shows great promise in clinic diagnostics and drug discovery applications, but also opens a novel perspective platform for bioanalysis.

DOI: 10.1021/acs.analchem.5b03661
Anal. Chem. XXXX, XXX, XXX−XXX

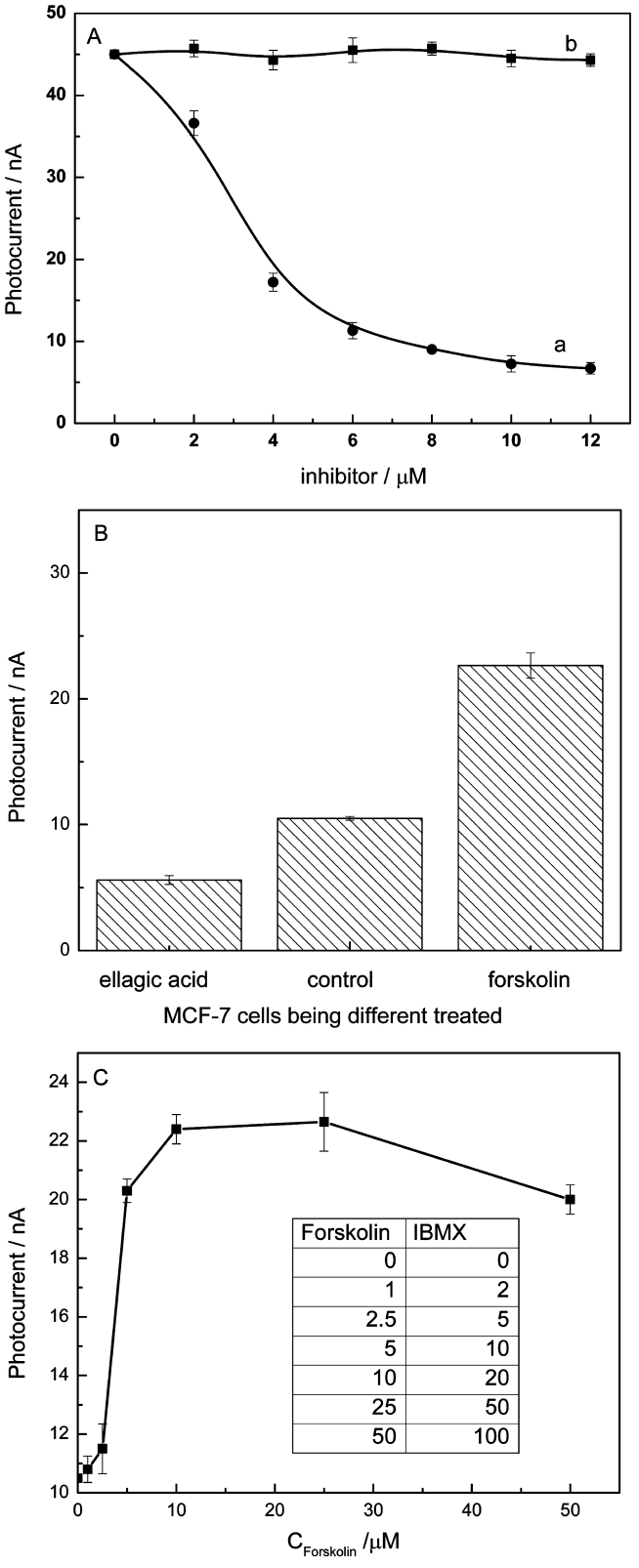

Figure 4. (A) Relationship between photocurrent responses and concentrations of ellagic acid (a) and Tyrphostin AG 1478 (b). The concentrations of PKA and ATP are 1 U mL^{-1} and 100 μM, respectively. (B) The PKA expression of MCF-7 cells treated with forskolin and ellagic acid. (C) The dependence of the photocurrent on different concentrations of forskolin and IBMX. The light power density is 190 mW cm^{-2}, the electrode area is 0.5 cm^2.

■ ASSOCIATED CONTENT

Supporting Information

The Supporting Information is available free of charge on the ACS Publications website at DOI: 10.1021/acs.analchem.5b03661.

Additional information (Figure S1−S6, and Table S1) (PDF)

■ AUTHOR INFORMATION

Corresponding Authors

*(Z.W.) Phone: 86-10-62798187; fax: 86-10-62771149; e-mail: wangzonghua@qdu.edu.cn.

*(Y.L.) E-mail: liu-yang@mail.tsinghua.edu.cn.

Notes

The authors declare no competing financial interest.

■ ACKNOWLEDGMENTS

This work was financially supported by the National Natural Science Foundation of China (NO. 21375073, 21235004, 21405086, 21475071, 21275082), the National Key Basic Research Development Program of China (973 special preliminary study plan, Grant no.: 2012CB722705), Tsinghua University Initiative Scientific Research Program (2014z21027) the Taishan Scholar Program of Shandong Province and the Natural Science Foundation of Qingdao (13-1-4-128-jch and 13-1-4-202-jch).

■ REFERENCES

(1) Kahn, B. B.; Alquier, T.; Carling, D.; Hardie, D. G. *Cell Metab.* **2005**, *1*, 15−25.

(2) Cox, J. S.; Shamu, C. E.; Walter, P. *Cell* **1993**, *73*, 1197−1206.

(3) Matsuoka, S.; Huang, M. X.; Elledge, S. J. *Science* **1998**, *282*, 1893−1897.

(4) Newton, K.; Dugger, D. L.; Wickliffe, K. E.; Kapoor, N.; de Almagro, M. C.; Vucic, D.; Komuves, L.; Ferrando, R. E.; French, D. M.; Webster, J.; Roose-Girma, M.; Warming, S.; Dixit, V. M. *Science* **2014**, *343*, 1357−1360.

(5) Cohen, P. *Curr. Opin. Chem. Biol.* **1999**, *3*, 459−465.

(6) Cho, H.; Mu, J.; Kim, J. K.; Thorvaldsen, J. L.; Chu, Q. W.; Crenshaw, E. B.; Kaestner, K. H.; Bartolomei, M. S.; Shulman, G. I.; Birnbaum, M. J. *Science* **2001**, *292*, 1728−1731.

(7) Musi, N.; Hirshman, M. F.; Nygren, J.; Svanfeldt, M.; Bavenholm, P.; Rooyackers, O.; Zhou, G. C.; Williamson, J. M.; Ljunqvist, O.; Efendic, S.; M?ller, D. E.; Thorell, A.; Goodyear, L. J. *Diabetes* **2002**, *51*, 2074−2081.

(8) Zhu, X. W.; Lee, H. G.; Raina, A. K.; Perry, G.; Smith, M. A. *Neurosignals* **2002**, *11*, 270−281.

(9) Sebolt-Leopold, J. S.; Herrera, R. *Nat. Rev. Cancer* **2004**, *4*, 937−947.

(10) Noble, M. E. M.; Endicott, J. A.; Johnson, L. N. *Science* **2004**, *303*, 1800−1805.

(11) Cohen, P. *Nat. Rev. Drug Discovery* **2002**, *1*, 309−315.

(12) Altai, M.; Orlova, A.; Tolmachev, V. *Curr. Pharm. Des.* **2014**, *20*, 2275−2292.

(13) Zhou, J.; Xu, X. H.; Liu, W.; Liu, X.; Nie, Z.; Qing, M.; Nie, L. H.; Yao, S. Z. *Anal. Chem.* **2013**, *85*, 5746−5754.

(14) Wang, Z. H.; Yan, Z. Y.; Sun, N.; Liu, Y. *Biosens. Bioelectron.* **2015**, *68*, 771−776.

(15) Liang, R. P.; Xiang, C. Y.; Zhao, H. F.; Qiu, J. D. *Anal. Chim. Acta* **2014**, *812*, 33−40.

(16) Liu, J. Q.; He, X. X.; Wang, K. M.; He, D. G.; Wang, Y. H.; Mao, Y. F.; Shi, H.; Wen, L. *Biosens. Bioelectron.* **2015**, *70*, 54−60.

(17) Deng, Z. Z.; Ye, M. L.; Bian, Y. Y.; Liu, Z. Y.; Liu, F. J.; Wang, C. L.; Qin, H. Q.; Zou, H. F. *Chem. Commun.* **2014**, *50*, 13960−13962.

DOI: 10.1021/acs.analchem.5b03661
Anal. Chem. XXXX, XXX, XXX−XXX

(18) Wang, Y.; Zhang, L.; Liang, R. P.; Bai, J. M.; Qiu, J. D. *Anal. Chem.* **2013**, *85*, 9148−9155.
(19) Li, T.; Liu, X.; Liu, D. J.; Wang, Z. X. *Anal. Chem.* **2013**, *85*, 7033−7037.
(20) Hou, T.; Wang, X.; Liu, X.; Lu, T.; Liu, S.; Li, F. *Anal. Chem.* **2014**, *86*, 884−890.
(21) Zhou, J.; Xu, X. H.; Liu, X.; Li, H.; Nie, Z.; Qing, M.; Huang, Y.; Yao, S. Z. *Biosens. Bioelectron.* **2014**, *53*, 295−300.
(22) Lin, L.; Liu, Y.; Zhao, X.; Li, J. H. *Anal. Chem.* **2011**, *83*, 8396−8402.
(23) Shen, Q. M.; Han, L.; Fan, G. C.; Abdel-Halim, E. S.; Jiang, L. P.; Zhu, J. J. *Biosens. Bioelectron.* **2015**, *64*, 449−455.
(24) Lu, W.; Jin, Y.; Wang, G.; Chen, D.; Li, J. H. *Biosens. Bioelectron.* **2008**, *23*, 1534−1539.
(25) Li, J.; Tu, W. W.; Li, H. B.; Han, M.; Lan, Y. Q.; Dai, Z. H.; Bao, J. C. *Anal. Chem.* **2014**, *86*, 1306−1312.
(26) Ma, Z. Y.; Ruan, Y. F.; Zhang, N.; Zhao, W. W.; Xu, J. J.; Chen, H. Y. *Chem. Commun.* **2015**, *51*, 8381−8384.
(27) Shen, Q. M.; Han, L.; Fan, G. C.; Zhang, J. R.; Jiang, L. P.; Zhu, J. J. *Anal. Chem.* **2015**, *87*, 4949−4956.
(28) Zhang, X.; Li, S.; Jin, X.; Zhang, S. *Chem. Commun.* **2011**, *47*, 4929−4931.
(29) Zhao, W. W.; Xu, J. J.; Chen, H. Y. *Chem. Soc. Rev.* **2015**, *44*, 729−741.
(30) Lu, W.; Wang, G.; Jin, Y.; Yao, X.; Hu, J. Q.; Li, J. H. *Appl. Phys. Lett.* **2006**, *89*, 263902.
(31) Chen, D.; Zhang, H.; Li, X.; Li, J. H. *Anal. Chem.* **2010**, *82*, 2253−2261.
(32) Zhang, X.; Xu, Y.; Yang, Y.; Jin, X.; Ye, S.; Zhang, S.; Jiang, L. *Chem. - Eur. J.* **2012**, *18*, 16411−16418.
(33) Tang, J.; Wang, Y.; Li, J.; Da, P.; Geng, J.; Zheng, G. *J. Mater. Chem. A* **2014**, *2*, 6153−6157.
(34) Li, C.; Wang, H.; Shen, J.; Tang, B. *Anal. Chem.* **2015**, *87*, 4283−4291.
(35) Fan, G. C.; Han, L.; Zhang, J. R.; Zhu, J. J. *Anal. Chem.* **2014**, *86*, 10877−10884.
(36) Tang, J.; Kong, B.; Wang, Y.; Xu, M.; Wang, Y.; Wu, H.; Zheng, G. *Nano Lett.* **2013**, *13*, 5350−5354.
(37) Wu, P.; Pan, J. B.; Li, X. L.; Hou, X. D.; Xu, J. J.; Chen, H. Y. *Chem. - Eur. J.* **2015**, *21*, 5129−5135.
(38) Wu, S.; Song, H.; Song, J.; He, C.; Ni, J.; Zhao, Y.; Wang, X. *Anal. Chem.* **2014**, *86*, 5922−5928.
(39) Ma, Z. Y.; Pan, J. B.; Lu, C. Y.; Zhao, W. W.; Xu, J. J.; Chen, H. Y. *Chem. Commun.* **2014**, *50*, 12088−12090.
(40) Zhao, W. W.; Chen, R.; Dai, P. P.; Li, X. L.; Xu, J. J.; Chen, H. Y. *Anal. Chem.* **2014**, *86*, 11513−11516.
(41) Fan, G. C.; Han, L.; Zhang, J. R.; Zhu, J. J. *Anal. Chem.* **2014**, *86*, 10877−10884.
(42) Roming, M.; Lunsdorf, H.; Dittmar, K. E.; Feldmann, C. *Angew. Chem., Int. Ed.* **2010**, *49*, 632−637.
(43) Cao, A. P.; Zhang, C. Y. *Anal. Chem.* **2012**, *84*, 6199−6205.
(44) Kakiage, K.; Aoyama, Y.; Yano, T.; Oya, K.; Kyomen, T.; Hanaya, M. *Chem. Commun.* **2015**, *51*, 6315−6317.
(45) Subramaniam, M. R.; Kumaresan, D. *ChemPhysChem* **2015**, *16*, 2543−2548.
(46) Hwang, S. H.; Song, H.; Lee, J.; Jang, J. *Chem. - Eur. J.* **2014**, *20*, 12974−12981.
(47) Kelly, K. L.; Coronado, E.; Zhao, L. L.; Schatz, G. C. *J. Phys. Chem. B* **2003**, *107*, 668−677.
(48) Mesch, M.; Zhang, C.; Braun, P. V.; Giessen, H. *ACS Photonics* **2015**, *2*, 475−480.
(49) Nishi, H.; Hiroya, S.; Tatsuma, T. *ACS Nano* **2015**, *9*, 6214−6221.
(50) He, P.; Liu, L.; Qiao, W.; Zhang, S. *Chem. Commun.* **2014**, *50*, 1481−1484.
(51) Zhao, W. W.; Tian, C. Y.; Xu, J. J.; Chen, H. Y. *Chem. Commun.* **2012**, *48*, 895−897.
(52) Zhao, W. W.; Yu, P. P.; Shan, Y.; Wang, J.; Xu, J. J.; Chen, H. Y. *Anal. Chem.* **2012**, *84*, 5892−5897.
(53) Kawawaki, T.; Takahashi, Y.; Tatsuma, T. *J. Phys. Chem. C* **2013**, *117*, 5901−5907.
(54) Wang, D.; Guo, L.; Huang, R.; Qiu, B.; Lin, Z.; Chen, G. *Electrochim. Acta* **2014**, *150*, 123−128.
(55) Yan, Z. Y.; Yang, M.; Wang, Z. H.; Zhang, F. F.; Xia, J. F.; Shi, G. Y.; Xia, L.; Y.H, L.; Xia, Y. Z.; Xia, L. H. *Sens. Actuators, B* **2015**, *210*, 248−253.
(56) Wang, M. J.; Sun, C. Y.; Wang, L. Y.; Ji, X. H.; Bai, Y. B.; Li, T. J.; Li, J. H. *J. Pharm. Biomed. Anal.* **2003**, *33*, 1117−1125.
(57) Si, P.; Ding, S. J.; Yuan, J.; Lou, X. W.; Kim, D. H. *ACS Nano* **2011**, *5*, 7617−7626.
(58) Liu, H.; Tian, Y.; Deng, Z. *Langmuir* **2007**, *23*, 9487−9494.
(59) Liu, H.; Zhang, X.; Zhai, T.; Sander, T.; Chen, L.; Klar, P. J. *Nanoscale* **2014**, *6*, 5099−5105.
(60) Da Silva, C. G.; Honeywell, R. J.; Dekker, H.; Peters, G. J. *Expert Opin. Drug Metab. Toxicol.* **2015**, *11*, 703−717.
(61) Xu, S. J.; Liu, Y.; Wang, T. H.; Li, J. H. *Anal. Chem.* **2010**, *82*, 9566−9572.

DOI: 10.1021/acs.analchem.5b03661
Anal. Chem. XXXX, XXX, XXX−XXX